On the Structure Sensitivity of CO_2 Hydrogenation over Cu/ZrO_2: Insights into the Role of the Support and the Active Sites

Tomás Vergara,* Daniel Gómez, Lucas Warmuth, Annika E. Enss, Martin Peterlechner, Rodrigo Pallacán, Vlad Martin Diaconescu, Laura Simonelli, Felix Studt, Patricia Concepción, Romel Jiménez, and Alejandro Karelovic*

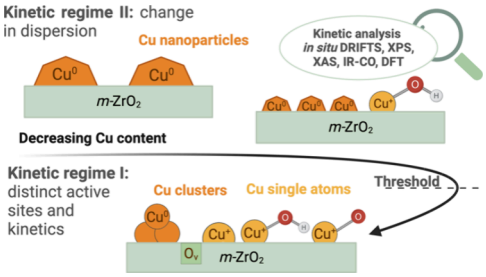

ABSTRACT: The well-known structure sensitivity of CO_2 hydrogenation to methanol has shown to be an impactful topic for the performance of the catalyst and yet remains unaddressed for Cu nanoparticles supported on ZrO_2, a material that has shown to be involved in the active site and the reaction mechanism of methanol formation. Herein, Cu/ZrO_2 catalysts were studied to unravel the underlying structure−activity relationships by combining surface and bulk characterization techniques, kinetic measurements, operando-DRIFTS and DFT calculations. Contrary to Cu over inert supports, the results showed different trends and two distinct kinetic regimes. For Cu nanoparticles larger than 2 nm, they are in accordance with previously reported results, this is, a change in the number of active sites, without affecting the nature of them. Conversely, it is demonstrated that the active sites are markedly different over the regime of nanoparticles smaller than 2 nm, accessed for ultralow Cu contents of 0.1 wt %, as evidenced from the systematic change of kinetic parameters and from operando-DRIFTS. The distinct active sites were identified as isolated Cu species (i.e., single atoms and Cu incorporated into the lattice of ZrO_2) and highly stable Cu clusters, both of which would allocate the formation of products for low metal contents. The results are certainly related to the interaction between Cu and ZrO_2 and unequivocally disclose the relationship between activity regimes and the nature of active sites as a function of the Cu particle size. Furthermore, they demonstrate that distinct active sites can be accessed just by varying the metal content on active reducible supports. As such, the findings are of particular relevance for the fundamental understanding of the interaction between Cu and ZrO_2 and its interdependence with the size of the Cu nanoparticles, as well as for the rational design of catalysts for CO_2 hydrogenation to methanol.

KEYWORDS: *CO_2 hydrogenation, Cu single atoms, operando-DRIFTS, structure sensitivity, ZrO_2-supported Cu*

1. INTRODUCTION

The synthesis of methanol from sustainable CO_2 and green hydrogen is a suitable alternative to the currently established process from syngas, as it would make it independent from fossil resources. Nevertheless, by increasing the concentration of CO_2 in the feed stream, unresolved challenges arise, mainly related to the lower carbon conversion and methanol selectivity as well as the higher concentration of water produced by the reverse water−gas shift reaction (r-WGSR). The previously mentioned challenges could be tackled, for instance, by employing ZrO_2 as a support, due to its hydrophobic properties, the abundance of Zr−OH groups, and its basic/acid sites.[1−16] In fact, ZrO_2 has shown to be involved in the active site of methanol synthesis at the interface with Cu nanoparticles,[4−6,13] where CO_2 would adsorb, while hydrogen will undergo dissociative adsorption over the copper surface.[2,13] Afterward, the reaction would follow the stepwise hydrogenation of formates (HCOO*) generated at the interface between Cu and ZrO_2.[1,5,6,13,14] In this sense, as of now, a consensus was attained regarding the nature of active sites and the reaction mechanism over Cu/ZrO_2. Nevertheless, besides the involvement of the support, the size of Cu nanoparticles has also shown to be impactful for CO_2 hydrogenation over inert supports.[17−19] Barberis et al.[17] studied the reaction over Cu/C catalysts with different particle sizes, evidencing that the turnover frequency (TOF) of both methanol and CO increased with the Cu diameter. The same observations arose from the works of Karelovic et al.[18] over Cu/SiO_2, van den Berg et al.[19] over Cu and CuZn, as well as from Visser et al.[20] and Simons et al.[21] for CO_2 methanation over Ni/SiO_2. Particularly, in the previously mentioned works, a ∼1 order of magnitude promotion of the TOF for methanol formation was observed, showcasing the importance of correctly assessing the effect of

the particle size for the design of new catalysts. The structure−activity relationships reported in these studies are attributed to the fact that the size of nanoparticles determines the relative amount between edges, corners, terraces, and step sites, which can thereafter define the reactivity of the catalyst.[22] This is the case for methanol and methane syntheses over inert supports and particles in the range 4−20 nm, from where, a change in the number of active sites was proposed to explain the results. Accordingly, it has been stated that methanol formation on Cu catalysts would preferentially take place over a specific active site, denominated B5.[18] Therefore, the structure sensitivity of CO_2 hydrogenation over Cu nanoparticles has been well-documented, even establishing a relationship between the trend exhibited by the TOF and the type of bond that is being activated (i.e., π or σ bond).[19,23] In this sense, Zhang et al.[24] proposed that the CO_2 activation is the structure-sensitive elementary step, as this molecule requires the coordination of more than one metal atom to react.[23] Nevertheless, these conclusions were obtained from studies over inert supports, and yet the topic remains unaddressed for ZrO_2-supported Cu nanoparticles, whose understanding is highly relevant for the rational design of new CO_2 hydrogenation catalytic materials.

Herein, Cu/ZrO_2 with different Cu concentrations were prepared (i.e., 0.1−10 wt %), resulting in Cu particle sizes in the range of 1−8 nm. The samples were analyzed from structural, kinetic, and IR-spectroscopic perspectives. Particularly, measurements of apparent orders of reaction with respect to CO_2 and H_2, as well as the H_2/D_2 kinetic isotope effect (KIE), were performed. Furthermore, operando-DRIFTS under steady-state and transient $H_2 \rightarrow CO_2/H_2$ were carried out to study the abundance and reactivity of the different intermediates. The surface and structure of the catalysts were analyzed by in situ and ex situ characterization techniques, namely, operando-XAS, XRD, XPS, and low-temperature IR-CO adsorption. The results showed that ultralow Cu contents over ZrO_2 lead to methanol and CO active sites of different nature, as evidenced from structural, kinetic, and spectroscopic perspectives. The nature of the Cu species was unequivocally differentiated between the samples and related to two separated kinetic regimes, one of them ascribed to the classical structure sensitivity reported over inert supports, which, in this case, is related to the number of Cu−Zr interfacial active sites, while for ultralow Cu contents, the surface is dominated by isolated Cu species and Cu clusters, certainly formed as a result of the metal−support interaction between Cu and ZrO_2.

2. MATERIALS AND METHODS

2.1. Catalyst Preparation. With the aim of studying the effect of ZrO_2-supported Cu particle size, five samples with different Cu contents (i.e., 0.1, 0.5, 1.0, 5.0, and 10.0 wt %) were prepared by modified wet impregnation with triethanolamine (TEA, Merck, 99%), as previously described in the literature.[25,26] Precursors of $Cu(NO_3)_2{\cdot}3H_2O$ (Merck, CAS no. 10031-43-3, 99.5%) and monoclinic zirconium oxide, m-ZrO_2, (Saint-Gobain Norpro, SZ 31163) were employed. In each case, 5 g of support, the corresponding amount of copper nitrate, and TEA in a TEA:Cu molar ratio equal to 2:1 were dissolved in 250 mL of distilled water and stirred for 30 min. The water was removed in a rotatory evaporator at 75 °C and later in an oven at 65 °C for 48 h. Thereafter, the samples were calcined in static air at 275 °C for 1 h (5 °C·min^{-1}) and subsequently reduced in a fixed bed reactor with a heating ramp rate of 5 °C·min^{-1} up to 400 °C. The later condition was maintained for 3 h in a flow of 50 $mL_{STP}{\cdot}min^{-1}$ of H_2 (Air Liquide 99.999%). Five different Cu-α catalysts were obtained, with α = 0.1, 0.5, 1.0, 5.0, and 10.0 wt %.

2.2. Catalyst Characterization. *2.2.1. Temperature-Programmed Reduction (H_2-TPR) and N_2O Chemisorption.* H_2-TPR experiments were performed in a ChemBET TPR/TPD (Quantachrome) equipment with ∼50 mg of calcined sample (400 °C, ramp rate of 5 °C·min^{-1}) between two quartz wool layers in a quartz U-reactor. Prior to the analysis, argon (Ar, Air Liquide 99.999%) was passed through the sample so that water or any adsorbed carbonaceous species could be removed from the surface. This procedure was performed at a flow rate of 30 $mL_{STP}{\cdot}min^{-1}$ and 400 °C (heating ramp of 5 °C·min^{-1}). Afterward, the H_2-TPR profiles were recorded in 30 $mL_{STP}{\cdot}min^{-1}$ of a H_2/Ar mixture (9.94 vol % H_2, Linde). The temperature was increased at a constant heating rate of 5 °C·min^{-1} from 20 to 400 °C. H_2 consumption was measured with a thermal conductivity detector (TCD). The H_2/Cu molar ratio was calculated from the hydrogen consumption and copper content in the catalysts. A Cu/SiO_2 catalyst, prepared following the same procedure previously described, was used as the calibration sample for the TCD signal.

Furthermore, with the aim of determining the Cu particle size in each sample, N_2O chemisorption experiments were performed. After the first H_2-TPR, the sample was cooled to 40 °C in Ar and, subsequently, a N_2O/Ar mixture (1.00 vol %, Linde) was flowed through the catalyst for 10 min (30 $mL_{STP}{\cdot}min^{-1}$). Then, a second H_2-TPR was recorded following the same procedure previously described. The number of exposed Cu atoms was estimated from the area under the H_2 consumption curve of the second TPR with Cu/SiO_2 calibration. The Cu dispersion and the particle size were thereafter calculated from eqs 2.1 and 2.2, respectively:

$$D = \frac{n_{Cu}}{m_{cat}{\cdot}X_{Cu}/M_{Cu}} \tag{2.1}$$

$$d_p = \frac{6(V_m/a_m)}{D} \tag{2.2}$$

where n_{Cu} corresponds to the moles of exposed Cu, m_{cat} to the mass of the catalyst used in each experiment, X_{Cu} to the mass fraction of Cu on the catalysts, M_{Cu} to the molecular weight of Cu, and V_m and a_m to the volume and surface area, respectively, of a single atom of Cu.

2.2.2. X-ray Diffraction (XRD). In order to study the crystalline structure of the catalysts, X-ray diffraction analysis was performed over Cu/ZrO_2-α catalysts on a Bruker AXS D4 diffractometer. The measurements were carried out with CuKα radiation (λ = 0.154 nm), 0.02°/s on a range between θ = 5° and θ = 90°.

2.2.3. Low-Temperature IR-CO Titration. The surface of the catalysts was analyzed by IR spectroscopy and CO titration at low temperature (IR-CO). The spectra were in situ recorded from a transmission homemade IR cell with KRS-5 (thallium-iodide bromide) windows in a Nicolet iS50 FTIR spectrometer with a DTGS detector and 4 cm^{-1} resolution. Before each measurement, the samples were reduced according to the previously described procedure (Section 2.2.1). Afterward, the system was evacuated (10^{-4} mbar) at a constant temperature for 1 h under dynamic vacuum and thereafter cooled to −160 °C. CO was progressively dosed, and the IR spectra were recorded.

2.2.4. X-ray Photoelectron Spectroscopy (XPS). XPS spectra from the ex situ-reduced samples were measured under vacuum

(10^{-9} mbar) and 25 °C with a PHOIBOS 150 MCD 9 analyzer. A monochromatic Alka α X-ray energy of 1486.60 eV was employed, and the analysis of the data was made with CasaXPS (Casa Software Ltd.) using the NIST library (NIST X-ray Photoelectron Spectroscopy (XPS) Database, version 3.5). The binding energies were corrected with respect to the C component at 284.6 eV.

2.2.5. X-ray Absorption Spectroscopy (XAS). XAS spectra were collected at the Cu K-edge (8978.9 eV) in fluorescence mode at the CLAESS beamline of the ALBA synchrotron.[27] The X-ray beam was monochromatized by means of the Si311 double-crystal monochromator, while the higher harmonics have been rejected by choosing appropriate coatings and angles of the collimating and focusing mirrors. Samples were in situ-reduced at 400 °C under H_2 flow (50 $mL_{STP}·min^{-1}$) for 1 h. Afterward, the catalysts were subjected to reaction conditions (260 °C, 8 bar, 5 $mL_{STP}·min^{-1}$ CO_2, 15 $mL_{STP}·min^{-1}$ H_2). XAS spectra were collected in isothermal mode at room temperature (RT), 400 °C (activation condition), 260 °C (under CO_2/H_2 reaction condition), and RT (after reaction). The products of the reaction were analyzed by mass spectrometry. The standards with well-defined oxidation states and local coordination were also measured (Cu foil, Cu_2O, and CuO). Standard procedures carried out using the Demeter package[27,28] have been employed to normalize the X-ray absorption near edge structure (XANES) and extract the extended X-ray absorption fine structure spectra (EXAFS). The Fourier transforms of the k^2 weighted EXAFS oscillations were performed over the k range of 2.7−11.2 $Å^{-1}$ with a Hanning window.

2.2.6. Transmission Electron Microscopy in Scanning Mode Coupled with Energy Dispersive X-ray Spectroscopy (STEM-EDX). For the analysis in transmission electron microscopy (TEM), samples were prepared by deposition onto Au-grids with a thin carbon film. High-angle annular dark-field scanning transmission electron microscopy (HAADF-STEM) coupled with energy dispersive X-ray spectroscopy (EDX) was conducted in an FEI Osiris instrument including a four-quadrant EDX detector operating at 200 kV. The data were denoised using principal component analysis, limiting possible components to less than 30. The EDX signal background and peak levels were used to estimate the detection limit.

2.3. Kinetic Measurements. Kinetic measurements were carried out in a stainless-steel fixed bed reactor (8 mm diameter). 200 mg of the undiluted catalyst (108−380 μm) were placed between two quartz wool sections, and the flow rates were controlled by mass flow controllers (Kofloc 8500). The system pressure was precisely adjusted by employing a back pressure regulator (Equilibar). The exhaust gases were analyzed with a gas chromatograph (SRI 8610C) equipped with a TCD, a flame ionization detector (FID), an FID with a methanizer, and a capillary column (30 m × 0.53 mm I.D. 1.0U MXT-WAX) and three packed columns (6′ × 1/8″ molecular sieve 5A, 18″ × 1/8″ Hayesep D and 6′ × 1/8″ Hayesep D). Before each experiment, in situ reduction of the catalyst was performed under H_2 (50 $mL_{STP}·min^{-1}$) at 400 °C (heating ramp of 5 °C·min^{-1}) for 1 h. Initially, the measurements were performed at 8 bar, 20 $mL_{STP}·min^{-1}$, a CO_2:H_2 molar ratio of 1:3, and four different temperatures (220, 240, 260, and 280 °C). The differential reactor conditions and the absence of strong transport limitations were confirmed from suitable methodologies.[25] In the same experimental apparatus, the H_2/D_2 kinetic isotope effect (KIE) (D_2 99.999%, Air Liquide) and the influence of the gas hourly space velocity (GHSV) were analyzed for Cu-0.1, Cu-1.0, and Cu-10.0 wt %. In both cases, methanol and CO formation rates were studied at 240 °C, 8 bar, and H_2:CO_2 = 3:1, under different total volumetric flows between 10 and 40 $mL_{STP}·min^{-1}$. In the case of the KIE, the results were extrapolated to zero residence time in order to obtain a measurement without the influence of the thermodynamic equilibrium and product readsorption. CO_2 and H_2 apparent orders of reaction of CO_2 and H_2 were estimated for the same catalysts at 8 bar and 240 °C by feeding different concentrations of reactants while keeping the total volumetric flow constant. N_2 (Air Liquide, 99.999%) was used to balance the concentrations. Iso-conversion conditions were ensured in order to compare the results.

2.4. Operando—Diffuse Reflectance Infrared Fourier Transform Spectroscopy (DRIFTS). Operando-DRIFTS experiments were carried out using a stainless-steel low dead volume cell with ZnSe windows on a Praying Mantis system (Harrick). A Nicolet 6700 FTIR instrument equipped with a liquid-nitrogen-cooled MCT-A detector was employed for IR analysis. The gases at the cell outlet were analyzed by using a Pfeiffer Vacuum mass spectrometer (Omnistar GSD320). A 4-way valve allows two different reaction systems to be connected to the cell and to easily switch between them. Back pressure regulators (Equilibar) were employed to precisely control the pressure in each of the available gas lines. Measurements were performed between 4000−400 cm^{-1}, with a sampling frequency of 0.251 s^{-1} and 10 scans per sample. For the measurements, H_2 (Air Liquide, 99.999%), CO_2 (AirGas, 99.99%), Ar (Air Liquide, 99.999%), and He (Air Liquide, 99.999%) were available. Steady-state and transient H_2/CO_2/Ar: 60/20/20 vol % → H_2/He/Ar: 60/20/20 vol % experiments were performed at 240 °C and 6 bar. Both the FTIR and MS signals were simultaneously analyzed.

2.5. DFT Calculations. The Vienna Ab Initio Simulation Package (VASP) version 5.4.1[29] together with the Atomic Simulation Environment (ASE)[30] were used to carry out DFT calculations with the Bayesian error estimation functional and van der Waals correction (BEEF-vdW).[31] A cutoff energy of 400 eV was employed. The model for the ZrO_2(101) surface was taken from previous work in our group.[32] It consists of periodic slabs with a thickness of three layers; the bottom layer was kept frozen during optimization. Different structures were calculated: copper species incorporated into the lattice of ZrO_2 ($Cu_{lattice}$) with a 3 × 3 ZrO_2 cell, as well as Cu−O and Cu−OH species with a 1 × 3 cell. For the CO vibrational analysis, a harmonic oscillator approximation was employed. Only the adsorbed CO molecule, the Cu atom, and the additional oxygen or OH-group were included into the vibration. CO vibrations were scaled by a factor of 1.0098 so that the calculated C−O stretching frequency of the gas phase molecule (2123.1 cm^{-1}) matches the experimental value (2144 cm^{-1}).

3. RESULTS AND DISCUSSION

The results from the characterizations performed over the different samples demonstrate that the Cu mean particle size increased with the metal content over the studied range of concentrations, which is a key aspect for the performance of structure sensitivity analysis. XRD showed features mainly assigned to the crystalline structure of monoclinic zirconia (m-)ZrO_2 (Figure S1). Only for high copper concentrations (i.e., Cu-5.0 and Cu-10.0%), a diffraction peak attributed to Cu crystals was identified, but this feature disappeared from Cu-1.0%, indicative of a change on the Cu dispersion as the metal

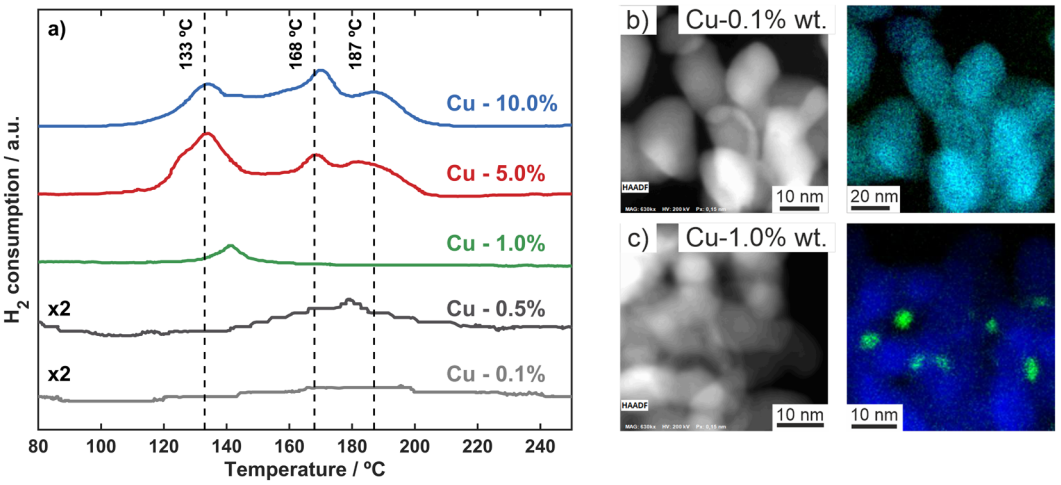

Figure 1. (a) H_2-TPR of the as prepared samples. Experimental conditions: 400 °C (5 °C·min^{-1}), 30 mL$_{STP}$·min^{-1}, and H_2/Ar (9.94 vol % H_2, Linde). The exhibited features are ascribed to highly dispersed Cu (133 °C), bulk of Cu nanoparticles (168 °C), and Cu interacting with ZrO_2 (187 °C). HAADF-STEM and EDX mapping of (b) Cu-0.1 wt % and (c) Cu-1.0 wt % after reduction. Green and blue correspond to the Cu and Zr elemental distribution, respectively. EDX maps were denoised by employing principal component analysis (PCA).

content decreases. On the other hand, H_2-TPR results (Figure 1a) show three distinct reduction features for the samples with 10.0 and 5.0 wt % at 133, 168, and 187 °C, ascribed to the reduction of highly dispersed copper nanoparticles, their bulk, and the Cu interacting with the ZrO_2 support, respectively.[12,25] The correspondence between the position of the peaks in these profiles suggests that Cu-10.0 and Cu-5.0 wt % exhibit copper sites of similar nature. Furthermore, the profile of Cu-5.0 wt % shows a higher relative intensity of the reduction feature at 133 °C, suggestive again of the improved dispersion of the metal over this sample in comparison to Cu-10.0 wt %. For lower Cu contents, the peaks at 168 and 187 °C disappear, while the peak at 133 °C shifts to higher temperatures. This behavior is indicative of a change in the degree of interaction between ZrO_2 and the highly dispersed Cu species for contents lower than 1 wt %. Qualitatively, the distinct Cu dispersion is also clearly evidenced between Cu-1.0 and Cu-0.1 wt % through STEM-EDX and the identification of Cu nanoparticles of ∼5 nm over Cu-1.0 wt % (Figure 1c). Meanwhile, the technique only depicts highly dispersed Cu species over Cu-0.1 wt % (Figure 1b). The results from STEM-EDX fall within the detection limit of the equipment, and the measurements for the rest of the samples are presented in Figure S2. Quantitatively, a second H_2-TPR was performed after N_2O chemisorption on the surface (i.e., H_2-TPR → N_2O → H_2-TPR, Figure S3). From it, the exposed number of Cu atoms was determined in each case (Table S1), which confirms that the size of nanoparticles is indeed changing over the studied range of concentrations, making the samples suitable for structure sensitivity analysis. The difficult identification of Cu nanoparticles from HR-TEM makes it impractical to obtain a particle size distribution based on this technique. Anyhow, the characterization results presented hereafter unequivocally confirm that the Cu particle size is increasing with the copper content , in direct agreement with Figure 1b,c, and reaffirm that the average value determined from N_2O chemisorption is a representative measure of the surface of the catalyst.

3.1. Structure Sensitivity over Cu/ZrO_2. Catalytic tests of CO_2 hydrogenation were performed under steady-state. Methanol and CO were the only detected products, and their concentrations were measured under differential reactor conditions and iso-CO_2 conversion as a function of temperature (Figures S4 and S5). The results normalized per mass of Cu are presented in Figure S6. Interestingly, it is evidenced that the formation rates of both products increase between the samples Cu-1.0 and Cu-0.1 wt %, specially at higher temperatures (i.e., 260 and 280 °C, Figure S6). Nevertheless, the rates remain almost unaffected from 5 to 10 wt %. The TOF per exposed copper atom for each product was estimated from the Cu particle size, as calculated from N_2O chemisorption experiments, considering that both products are formed following parallel pathways (Figure 2a,b). A consecutive r-WGSR + CO hydrogenation mechanism was discarded for methanol based on thermodynamic considerations, following a method previously described in the literature (Figure S7).[33−35] For methanol (Figure 2a), the results show that the TOF is sensitive to the structure of the catalyst, with an increasing trend between ∼1 and ∼2 nm (i.e., indicated as Regime I in Figure 2a), which then turns to decreasing (i.e., indicated as Regime II in Figure 2b). Even if the former could seem contradictory when compared to the higher formation rate for Cu contents lower than 1.0 wt % (Figure S6), it implies a trade-off between less active methanol sites and their amount per gram of Cu in the catalyst, resulting in a positive net effect. This is supported by the stepped increase in the apparent activation energies for methanol formation over Cu particles of less than 2 nm (Figure 2c). According to its definition from a Langmuir−Hinshelwood perspective, a change in this parameter can be either attributed to an energetic modification of the rate-determining step (RDS) itself, or to a change in the coverage of intermediates at the surface of the catalyst. In any case, both the modification of the TOF_{CH3OH} slope and of the apparent activation energy indicate a modification of the nature of methanol active sites for smaller nanoparticles. A similar behavior has been previously reported in the literature for Cu supported on ZnO[36] and Al_2O_3. Moreover, it is evidenced from Figure 2a that the TOF_{CH3OH} over Cu/ZrO_2 is different than over Cu/SiO_2 measured under the same reaction conditions, both qualitatively and quantitatively, therefore reaffirming that the nature of the active sites for methanol over Cu/ZrO_2 is distinct than over SiO_2.[37] This phenomenon cannot be explained solely by the difference in the surface of exposed copper and claims that ZrO_2 is directly involved in the reaction mechanism.[38] In this sense, the interface

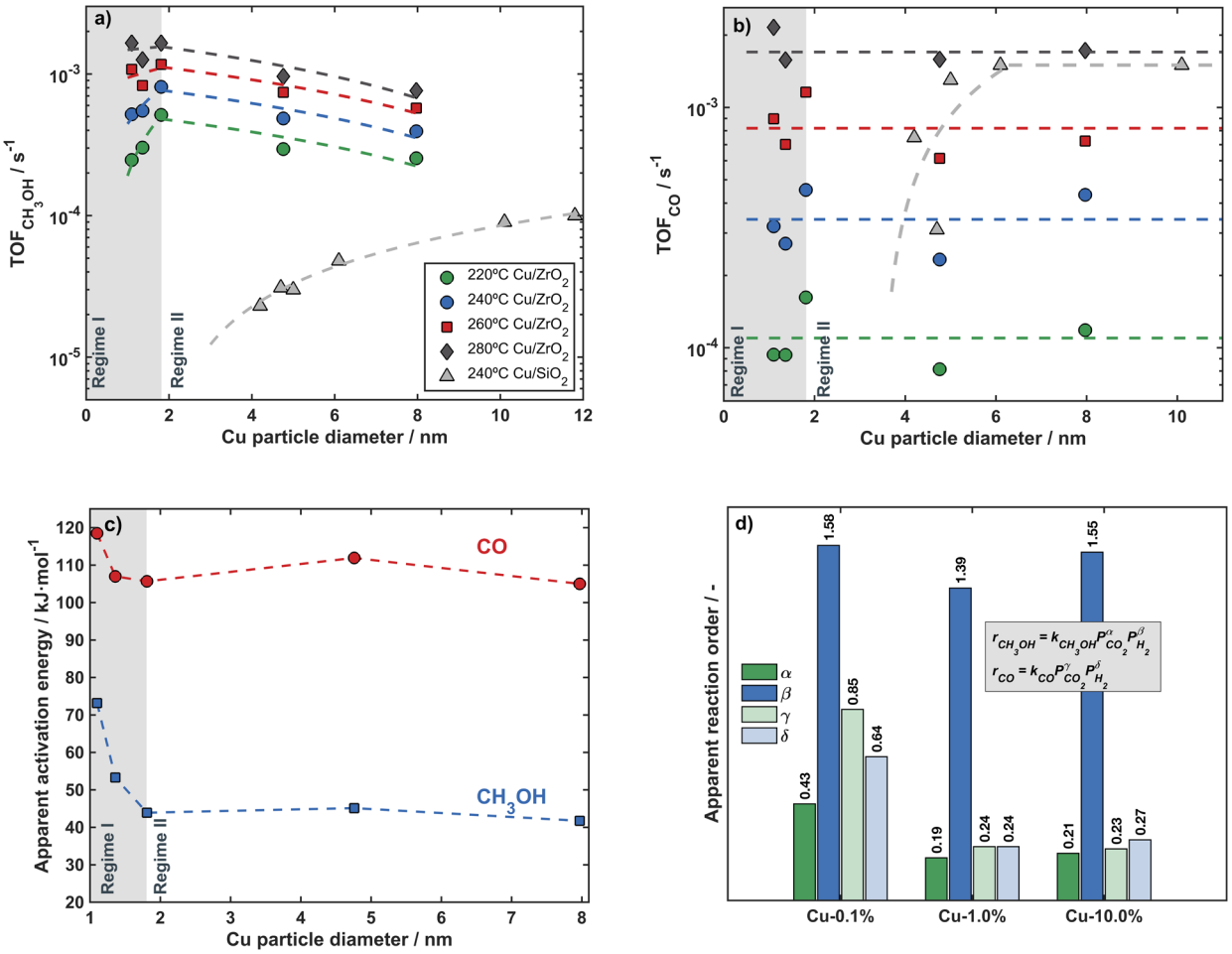

Figure 2. Turnover frequency of (a) CH_3OH and (b) CO formation as a function of the Cu particle diameter and temperature over Cu/ZrO_2 and Cu/SiO_2. The values were obtained after normalization of the formation rates by the number of Cu sites, determined by N_2O chemisorption. Cu/SiO_2 experimental results were measured for a previous work under the same conditions as in this study. Reproduced or adapted with permission from ref 18. Copyright 2024 Elsevier. (c) Apparent activation energies as a function of the Cu particle diameter. P = 8 bar, CO_2/H_2: 25/75 vol %, 20 $mL_{STP}·min^{-1}$. Lines are drawn to guide the eye. (d) CO_2 and H_2 apparent reaction orders for CH_3OH and CO as a function of Cu content. P = 8 bar, T = 240 °C, CO_2/H_2: 25/75 vol %, 20 $mL_{STP}·min^{-1}$. α and γ correspond to the apparent orders of reaction with respect to CO_2 for methanol and CO, respectively, while β and δ correspond to the apparent orders of reaction with respect to H_2 for methanol and CO, respectively.

between Cu and ZrO_2 has been repeatedly reported as the methanol active site over these materials.[1,9,12] A closer comparison with the literature is presented in Figure S8, where it is further evidenced that the structure sensitivity over Cu/ZrO_2 is manifested in a different trend than over other inert and active materials and that this work sheds light over a region of smaller nanoparticles that has not been analyzed so far.

On the other hand, the TOF_{CO} as a function of the Cu particle size is presented in Figure 2b, from where no structure sensitivity is detected over ZrO_2, in contrast with the results from Cu/SiO_2 which depict an increasing trend from particle sizes of ∼4 nm onward. The differences are only observed over Regime I, while the quantitative and qualitative similitudes of the TOF_{CO} between ZrO_2 and SiO_2 over Regime II (Figure 2b) suggest that the active sites for the formation of CO are, to some extent, equal among the two supports in this range of particle sizes. Therefore, similarly to the interpretation for methanol results, it is suggested that Cu contents lower than 1.0 wt % would allow to access new active sites, which, in turn, would result in a different structure−activity relationship and a slight increase of the CO-apparent activation energy, as observed from Figure 2c.

The apparent orders of reaction with respect to both reactants are presented in Figure 2d over Cu-10.0, Cu-1.0, and Cu-0.1% wt. For methanol formation, the results show a 2-fold increase in this parameter with respect to CO_2 for Cu-0.1 wt % in comparison to Cu-1.0 and Cu−10−0 wt %. In order to get further insights from this information, the results will be leveraged from a Langmuir−Hinshelwood perspective, as presented in the following equation:

$$r_{CH_3OH} = \frac{k_{CH_3OH} P_{CO_2}^{x} P_{H_2}^{y} (1 - \eta_{CH_3OH})}{(1 + \sum \theta_{int} \theta_{*}^{-1})^2} \quad (3.1)$$

where η_{CH_3OH}, θ_{int}, and θ_* correspond to the approach to equilibrium of methanol synthesis, the coverage of intermediates, and the coverage of active sites, respectively, while x and y can be interpreted as the number of CO_2 and hydrogen molecules involved in the RDS of the reaction, respectively. Since there will be always one CO_2 molecule taking part in the formation of methanol, the increase of the CO_2-apparent order can only be explained by a diminution of the coverage of CO_2-related intermediates over methanol active sites (i.e., θ_{int}). On the contrary, the H_2 apparent reaction order remains

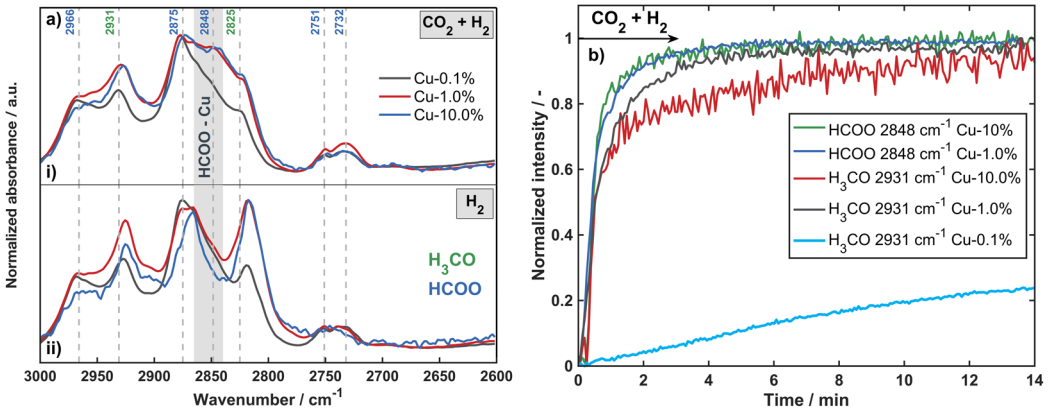

Figure 3. (a) Steady-state FTIR spectrum in the C−H vibration region (2600−3000 cm^{-1}) for Cu-0.1, Cu-1.0, and Cu-10.0 wt % normalized according to the highest intensity (i) before and (ii) after the switch $CO_2/H_2 \rightarrow H_2$. (b) Transient time-evolution of FTIR signals of methoxy and formate species after the switch of $H_2 \rightarrow CO_2/H_2$. P = 6 bar, T = 240 °C, 25 $mL_{STP}{\cdot}min^{-1}$, H_2/CO_2(He)/Ar = 60/20/20 vol %.

approximately constant, which can be rationalized in two ways: (i) the coverage of hydrogenated methanol intermediates changes in the same manner as the order in the numerator of the kinetic expression (i.e., $\Delta\theta_{int} \approx \Delta y$), therefore avoiding an appreciable net effect, or (ii) the intermediates for which the coverage is changing correspond to molecules that do not possess hydrogen in its structure (e.g., carbonates). Nevertheless, for either of the previous hypotheses, the phenomenon is consistent with the change in the CO_2 apparent order of CO_2 and is likely the result of different active sites for lower Cu contents, in fair agreement with the previous discussion.

Likewise, both apparent orders of reaction for CO formation increase as the Cu content goes lower than 1.0 wt %, ∼4 and ∼3-fold with respect to CO_2 and H_2, respectively (Figure 2d). The formation of CO has been reported to take place following a hydrogen-assisted mechanism through carboxyl species over Cu active sites.[35,39] From eq 2.1, the reactant orders in the numerator of the kinetic expression for this reaction mechanism will always be equal to 1 and 0.5 for CO_2 and H_2, respectively. Therefore, the observed changes in the apparent orders of reaction for CO formation can only be attributed to a decrease in the coverage of intermediates or to a change in the reaction mechanism. These evidence reaffirms that, like for methanol, the nature of the CO active sites drastically changes for Cu contents lower than 1.0 wt %.

The H_2/D_2 kinetic isotope effect (KIE) was measured as a function of the residence time (Figure S9). Since the analyses were performed under differential conditions, the contribution from the thermodynamic isotope effect (TIE) can be neglected.[40] Furthermore, the results do not show a dependence on the residence time, and as such, they are representative of the phenomena under the absence of product readsorption for the forward reaction only. The KIE for methanol is inverse for all the studied catalysts but less significant over Cu-0.1 wt %, which exhibits a ∼2-fold higher value in comparison to Cu-1.0 and 10.0%, irrespective of the residence time. The trend, analogous to the change in the apparent orders of reaction, suggests a distinct RDS or coverage of intermediates for Cu-0.1 wt %, now from an isotopic perspective. This phenomenon is consistent with the formation of Cu active sites of distinct nature over this sample, which would consequently result in a different hydrogen dissociation capability or distinct hydrogenation of intermediates, thereafter producing an increase in the KIE.

The particular behavior for Cu-0.1 wt % evidenced from kinetic measurements and mechanistic considerations is also observed from the study of the catalyst's surface via operando-DRIFTS (Figure 3). Figure 3a, panel i, presents the results under CO_2/H_2 steady-state, while the information over the bare m-ZrO_2 support is depicted in Figure S10. A close agreement between the normalized curves of Cu-1.0 and Cu-10.0 wt % is evidenced. The band at 2966 cm^{-1} has been ascribed to δ(CH) + ν_{as}(OCO) vibrations (i.e., combination of C−H and O−C−O vibrations[2,41−44]), while the one at 2875 cm^{-1} would correspond to the stretching ν_s(CH) vibrations of bidentate formates over ZrO_2.[6,45] The signals at 2931 and 2825 cm^{-1} were previously related to $\nu_{as}(CH_3)$ and $\nu_s(CH_3)$ of methoxy species, respectively,[43,46] and the one at 2732 cm^{-1} to δ(CH) + ν_s(OCO) of formates.[47] On the other hand, the band at 2848 cm^{-1}, which completely disappears under He/H_2 conditions (Figure 3a, panel (ii)), is ascribed to formate species that would take part in the reaction mechanism of methanol formation and that has been related to the C−H vibration feature over Cu near ZrO_2.[6,45] The resemblance between the ratio of the peaks and their position under CO_2/H_2 and He/H_2 conditions is indicative that both the nature and coverage of intermediates are equal among Cu-1.0 and Cu-10.0% catalysts, consistent with the correspondence between the apparent orders of reaction and the discussion from it (Figure 2d). Nonetheless, the results are different for Cu-0.1%, from where two insights can be withdrawn: (i) qualitatively, the relative concentration of intermediates is lower on this sample, particularly for formates at 2848 cm^{-1} which are not detected (Figure 3a, panel (i)) and (ii) the proportion between active formates (i.e., 2848 cm^{-1}) and methoxy species is different in this case compared to the other catalysts (i.e., ratio between active formates (2848 cm^{-1}) and methoxy species (2931 cm^{-1}) is ∼1.2 for Cu-10.0% and ∼1 for Cu-0.1%). Both observations demonstrate that the coverage and nature of intermediates are different over this sample, as stated from the previous kinetic discussion. Furthermore, they reaffirm the hypothesis that the nature of the predominant active sites will change for Cu contents lower than 1.0% wt. and allow to relate the activity over Regime II (Figure 2a) to the 2848 cm^{-1} formate species, while for Cu-0.1 wt %, methanol synthesis would likely take place following the hydrogenation of a different intermediate, not detected by operando-DRIFTS. The intermediacy of formates over Cu−Zr interfacial sites for methanol synthesis has been previously reported in the literature and is

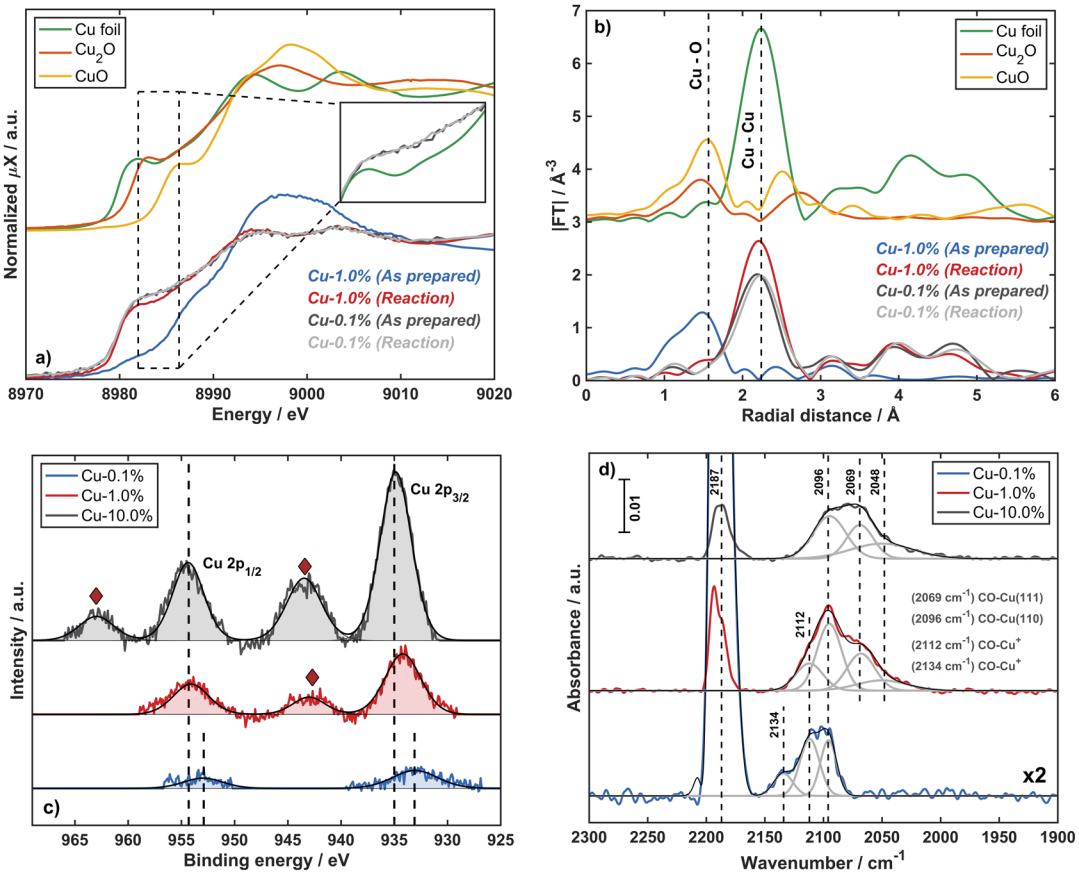

Figure 4. (a) Normalized Cu K-edge XANES and (b) Fourier transforms of the corresponding k^2 weighted EXAFS oscillations for Cu-0.1 and Cu-1.0% catalysts after ex situ reduction (as prepared) and in situ reduction and reaction (reaction), compared with the references (Cu^0, Cu_2O, and CuO). H_2/CO_2: 75/25 vol %, 8 bar, 260 °C. (c) XPS spectra of Cu 2p over Cu-0.1, 1.0, and 10.0 wt % after ex situ reduction following the procedure described in the methodology section. (◆) correspond to the satellite peaks of Cu $2p_{1/2}$ and Cu $2p_{3/2}$. (d) IR-CO adsorption over Cu-0.1, 1.0, and 10.0 wt % under 0.08 mbar of $CO_{(g)}$ at $T = -160$ °C. Detected vibrations at 2187, 2134, 2112, 2096, 2069, and 2048 cm^{-1} are attributed to CO-Zr^{4+}, CO-Cu^+, CO-Cu(110), and CO-Cu(111), respectively.

consistent with the findings from this work for Cu-1.0 and Cu-10.0 wt %.[1,5,6,13,14]

Operando-DRIFTS results were additionally leveraged from the reactivity of intermediates, which was assessed from the transient evolution of formates (2848 cm^{-1}) and methoxy (2931 cm^{-1}) signals after the switch $He/H_2 \rightarrow CO_2/H_2$ (Figure 3b). Formates over Cu-0.1% are not presented in Figure 3b since they were not detected over this sample. A close qualitative consistency is again evidenced among formates for Cu-10.0 and Cu-1.0%, as well as for methoxy species. Additionally, the order in which the different signals evolve reaffirms that the reaction mechanism for methanol formation takes place through the stepwise hydrogenation of formates at the corresponding active sites. For Cu-0.1% instead, the methoxy signal shows a much slower evolution, achieving only 20% of the final steady-state after 14 min. The contrast can be assessed quantitatively from the initial slope of each curve, which exhibits differences of at least 1 order of magnitude between Cu-1.0 and Cu-0.1% (i.e., k'_{CH_3O} equal to 0.27 and 0.02 s^{-1}, respectively). The distinct apparent constants of reaction (k'_{CH_3O}) for methoxy formation are consistent with a change in the hydrogenation capability as evidenced from the measurement of the KIE and indicates that the turnover frequency on Cu-0.1 wt % is slower, in fair agreement with the results from Figure 2a. Moreover, according to the quasi-steady-state approximation and the Langmuir–Hinshelwood formalism, the apparent reaction constant for methoxy formation is defined as $k'_{CH_3O} = k_{CH_3O}\theta_{CH_2O}\theta_H$. Therefore, the contrasting trends in Figure 3b could be attributed to a modification of the kinetic constant of that elementary step, a change in the coverage of the involved intermediates, or both. Anyhow, the results are in line with the distinct nature of methanol active sites over Cu-0.1 wt %, as evidenced from kinetic and IR-spectroscopic perspectives.

Previous works advocated to the structure sensitivity of methanol synthesis over Cu catalysts have also reported changes in the TOF with the particle size and postulated that the results could be explained by either of the following reasons[48−50]: (i) size-dependent interactions between metal and support, (ii) electronic effects related to the particle size, or (iii) structure sensitivity of the reaction itself, related only to the number of active sites. Barberis et al.[17] and Karelovic et al.[18] studied the CO_2 hydrogenation to methanol over Cu catalysts supported on inert materials and discarded that one of the two former alternatives could explain their results. Therefore, they considered the latter as the underlying phenomena behind the observed change in activity. The authors demonstrated that the apparent activation energy remained constant and that the change in the TOF was attributed to a modification of the pre-exponential factor in the kinetic constant, directly related to the number of active sites and not to their nature. This is consistent with the results from the previously defined Regime II in Figure

2, as well as with the IR-spectroscopic information over Cu-1.0 and Cu-10.0 wt % (Figure 3), and allows to conclude that the phenomenon is analogous to the one described over Cu/SiO_2[18] and Cu/C.[17] In this case, the trends over Regime II could be related to a change in the number of Cu−Zr interfacial sites, previously reported as the methanol active sites.[4−6,13] In contrast, Regime I over Figure 2 and the IR-spectroscopic information from Cu-0.1 wt % are not compatible with the previous arguments. In this sense, the evidenced change in activity would likely be the result of the metal−support interactions between Cu and ZrO_2, or of electronic effects, which have been reported for Cu particles smaller than 3 nm and hence cannot be discarded here.[48,49,51] Interestingly, Cu-0.1 wt % shows a markedly distinct behavior in Figures 2 and 3, even though the difference in Cu concentration is the same between all three samples (i.e., 10-fold), suggesting that only ultralow copper contents allow access to the distinct kinetic regime.

3.2. Identification of Active Sites. In order to gain further insights from the structure of the catalyst and its interplay with the obtained kinetic and spectroscopic results, low-temperature IR-CO adsorption, XPS and operando-XAS were performed. Figure 4a,b shows the Cu K-edge X-ray absorption spectra collected in situ over Cu-0.1 and Cu-1.0 wt %, specifically for the as prepared and after reaction samples. XANES spectra and the Fourier transform of the k^2 weighted EXAFS oscillations are reported in Figure 4a,b, respectively.

Both XANES and EXAFS demonstrate that Cu-1.0 wt % is initially oxidized and exhibits a local environment in accordance with the CuO reference. Thereafter, as expected from the reduction/reaction, the local environment drastically shifts to a predominance of reduced Cu^0. On the contrary, Cu-0.1 wt % is not affected by the reduction/reaction treatments, and the sample remains mainly as metallic Cu. This distinct behavior reaffirms that the nature of copper species is different for low metal contents, in fair agreement with the information from the kinetic and spectroscopic analyses. Interestingly, the edge for Cu-0.1 wt % exhibits slight differences with respect to the Cu foil reference, which further suggests the existence of Cu species with higher oxidation state over this sample (Figure 4a, inner box). Moreover, EXAFS reaffirms that the particle size changes with the reduction/reaction treatment over Cu-1.0 wt %, while for Cu-0.1%, it remains unaffected, and it further indicates that the Cu diameter is different between both samples as shown by the maximum intensity of the FT-EXAFS at 2.25 Å (Figure 4b), in accordance with N_2O chemisorption and STEM-EDX (Figure 1b,c). The results generally indicate that Cu species over Cu-0.1 wt % are highly stable after reduction/reaction and consist of a mixture of Cu^0 and Cu^+ oxidation states, in contrast to Cu-1.0 wt %, which exhibits a change in the local environment.

XPS spectra of the ex situ-reduced samples are depicted in Figure 4c. The quantitative information issued from the analysis of the spectra is presented in Tables S2 and S3. The results over O 1s and Zr 3d do not show differences among the different catalysts (Figure S11). The spectra from Cu-10.0 and Cu-1.0 wt % exhibit satellite peaks for $2p_{1/2}$ and $2p_{2/3}$ features (Figure 4c), which are indicative of the Cu^{2+} oxidation state on the surface of the catalyst, probably formed after the ex situ reduction and subsequent oxidation of Cu sites.[52−54] The satellites gradually disappear as the Cu content decreases, which is accompanied by a shift of the Cu $2p_{1/2}$ and Cu $2p_{3/2}$ features to lower binding energies. The absence of satellites for Cu-0.1 wt % indicates that this sample keeps its surface oxidation state after contact with air, which showcases once more the higher stability of Cu species on this catalyst, in fair agreement with the evidence from XANES. Furthermore, it is well-known that the study of the Cu surface by XPS needs to account necessarily for the results of binding energy, kinetic energy, and Auger peak from the Cu 2p spectra. These parameters can be related among them through a Wagner plot, as previously reported in the literature for Cu/ZrO_2 materials.[54] The results obtained for the catalysts of this work are presented in Table S3, and their values are in fair agreement with the previously indicated switch in the nature of Cu species from Cu^+ to Cu^{2+} between Cu-0.1 wt % and the other samples, respectively (Figure 4c). It is important to note that the magnitude of the shifts in binding energy and modified Auger parameter between Cu-1.0 and Cu-10.0 wt % falls within the reported range for a change in Cu dispersion over CuO/ZrO_2,[54] indicating that the Cu particle size would be the main distinction among these samples, in accordance with their previously observed kinetic and mechanistic resemblance. On the contrary, the differences among Cu-0.1 wt % and the other two samples are higher than the reported values attributed to the solely modification of the particle size,[54] which is consistent with Cu-0.1 wt % exhibiting active sites of distinct nature and with the discussed kinetic and IR-spectroscopic differences.

The results from IR-CO adsorption are presented in Figure 4d for Cu-10.0, Cu-1.0, and Cu-0.1 wt % under 0.08 mbar of $CO_{(g)}$ at −160 °C. Additionally, for comparison purposes, the spectrum over pure m-ZrO_2 is depicted in Figure S12. The results show vibrations attributed to the adsorption of CO over Cu and Zr. The feature at 2187° is ascribed to CO-Zr^{4+}, as this band is also clearly visible over the spectrum of the bare support. On the other hand, the features at 2134 and 2112 cm^{-1} evidenced for Cu-0.1 wt % would correspond to CO-Cu^+ species,[55] and the difference in the wavenumber among them would be ascribed to a distinct local structure and consequent different formal charge for each site. The vibration bands at 2096 and 2069 cm^{-1} have been related to CO adsorbed on Cu(110) and Cu(111), respectively.[55−59] In order to verify this assignment and further study the nature of the Cu sites in each catalyst, DFT calculations were performed for CO adsorption on different model systems representing Cu atoms adsorbed onto or incorporated into the lattice of ZrO_2. The calculated C−O vibrations suggest three possible systems that match the experimentally observed peaks over Cu-0.1 wt %, as shown in Figure 4d. The vibration feature at 2134 cm^{-1} can be assigned to a Cu atom incorporated into the lattice of ZrO_2 (Figure 5a,d), which results in a calculated vibrational frequency of 2136 cm^{-1}. This system was structured after the direct replacement of Zr^{4+} by Cu^{2+} and the removal of an adjacent O^{2-} atom to account for charge balance. The ability of ZrO_2 to incorporate copper atoms into its lattice has been previously reported in the literature and is consistent with the findings from this work.[60] On the other hand, Cu single atoms adsorbed on ZrO_2 are not stable by themselves but can be anchored to the surface by an O^{2-} atom or an OH^- group (Table S4). The Cu−O−CO species (Figure 5b,e) shows a CO vibration frequency of 2114 cm^{-1}, in fair agreement with the 2112 cm^{-1} feature detected experimentally over the Cu-0.1 and Cu-1.0 wt % samples. Cu−OH−CO species were also analyzed (Figure 5c,f), which resulted in a CO vibrational frequency of 2097 cm^{-1}. While formally these systems represent two Cu^{2+} species ($Cu_{lattice}$−CO, Cu−O−CO) and one Cu^+ species (Cu−OH−CO), the performed Bader charge analysis (Figure S13) indicates that the oxidation state of the Cu atoms is in the

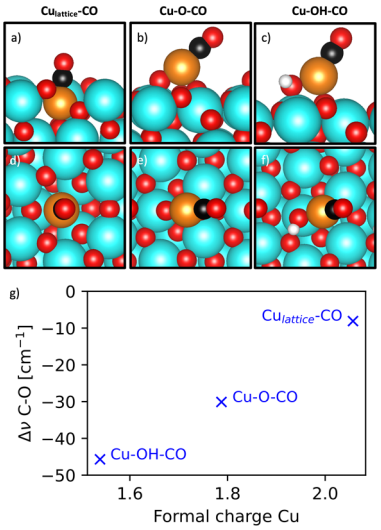

Figure 5. (a)−(c) Side view and (d)−(f) top view of model structures $Cu_{lattice}$−CO, Cu−O−CO, and Cu−OH−CO, respectively. Color code: red = O, black = C, white = H, orange = Cu, and turquoise = Zr. (g) Calculated C−O vibration frequencies relative to calculated formal charge. Charges were determined by Bader charge calculation (see Figure S13 for more details).

range of +1.5 to +2.1 (Figure 5g), with the vibrational frequency increasing with higher charge.

From the combined results of IR-CO adsorption and DFT calculations, it is stated that the nature of Cu species on the surface gradually shifts as the metal content increases, going from a catalytic surface where mainly Cu single atoms and Cu species incorporated into the lattice of ZrO_2 coexist over Cu-0.1 wt %, to a predominance of metallic Cu (i.e., Cu(110)) on Cu-1.0 wt %, to a metallic Cu structure where different crystalline facets (i.e., Cu(110) and Cu(111)) arise on Cu-10.0 wt %. Quantitatively, the change in the nature of Cu species between Cu-0.1 and Cu-1.0 wt % can be assessed, for instance, from the decrease in the relative amount of Cu single atoms related to the vibration feature at 2112 cm^{-1} (i.e., 44% for Cu-0.1 wt % and 19% for Cu-1.0 wt %), therefore indicating that these Cu sites would be predominately accessed only for ultralow Cu contents. Moreover, this CO vibration is not detected over Cu-10.0 wt %, suggesting that the concentration of single atoms over Cu-1.0 wt % is not high enough to produce an appreciable kinetic difference between these two catalysts. On the other hand, the band at 2096 cm^{-1} matches both the calculated assignment to Cu single atom and the reported correspondence to Cu(110). According to the absence of evident Cu nanoparticles over Cu-0.1 wt %, as observed from STEM-EDX (Figure 1b), it is proposed that this feature would correspond to single atoms over Cu-0.1 wt %, while the band would mainly correspond to the Cu(110) facet of the nanoparticles that are formed as the concentration of Cu increases for Cu-10.0 wt %. Likewise, the change in the relative amount of the distinct facets of Cu^0 reaffirms once more that the size of the nanoparticles is changing with the copper content.

The distinct features evidenced from IR-CO adsorption are consistent with the results from XPS, which indicated that the nature of the surface Cu species present over Cu-0.1 wt % is drastically different than over the other samples. To account for the highly stable nature of metallic Cu species and Cu−Cu bonds over XANES and EXAFS for Cu-0.1 wt %, it is suggested that the surface of this catalyst would additionally be composed by highly stable Cu clusters (i.e., arrangement of ∼3 atoms of Cu) which, due to their size or to the low Cu content, would not be identified by STEM-EDX. The fact that the contribution from Cu^+ species is barely detected at the Cu K-edge of Cu-0.1 wt % (Figure 4b) suggests that its surface density is low, as expected from the 0.1 wt % Cu loading over this sample. Likewise, it must be considered that, while XAS is a bulk sensitive technique, XPS and IR probe the surface of the catalysts, where Cu-isolated species are formed.

In summary, the results from these characterizations are consistent with the two kinetic regimes previously described since: (i) for Cu contents higher than 1.0 wt %, there is a change in the relative abundance of Cu facets with no modification of the nature of the main methanol active sites (Figure 4d). XPS confirms that this phenomenon is only attributed to the higher Cu dispersion exhibited by Cu-1.0 wt % (Regime II, Figure 1), with single atoms not being abundant enough to have an appreciable kinetic impact over this sample (Figure 2); (ii) for Cu contents lower than 1.0 wt %, IR-CO adsorption, XPS, and XAS consistently show the generation of Cu sites of different nature, particularly Cu-isolated atoms and highly stable Cu clusters, which would result in the observed unalike kinetic behavior (Regime I). Consequently, it is concluded that the new active sites accessed for ultralow Cu contents over ZrO_2 would be able to allocate the formation of both relevant products, strongly affecting the performance of the catalyst and contrasting with the previously reported structure−activity trends over inert supports.

4. CONCLUSIONS

Cu/ZrO_2 samples with different Cu particle sizes were prepared and analyzed from structural, kinetic, and operando IR-spectroscopic perspectives. The results contrasted with previous trends over inert supports, showcasing that ZrO_2 impacts the reported structure-sensitivity of Cu nanoparticles. Furthermore, they evidenced two distinct regimes for methanol and CO formation: (i) a region of average particle sizes >2 nm (Cu contents >1.0 wt %) where the methanol TOF decreases without exhibiting a change in the kinetic parameters and the IR-spectroscopic spectrum and (ii) a region of particle sizes <2 nm (Cu contents <1.0 wt %) where the methanol TOF increases at a different rate with a modification of the measured information. The former was found to be consistent with the classical structure sensitivity reported for Cu nanoparticles over inert materials, and in this case would be related to a change in the number of Cu−Zr and Cu active sites for methanol and CO, respectively, without affecting the nature of them. Nevertheless, for smaller nanoparticles, the results were consistent with a change in the nature of the active sites for both products, certainly as a result of the metal−support interaction. This was evidenced by the systematic modification of the apparent activation energy, apparent orders of reaction, KIE, nature and coverage of intermediates, and reactivity of methoxy species. Further characterizations combined with DFT calculations demonstrated that the formation of isolated Cu sites (i.e., single atoms and Cu incorporated into the lattice of ZrO_2) and highly stable Cu clusters would dominate the surface of the catalyst for ultralow Cu contents and would be responsible for the evidenced kinetic and IR-spectroscopic contrasts.

The conclusions from this work highlight the importance of tackling the structure−activity relationships for the rational design of methanol catalysts over supports that participate in the reaction mechanism and in the active site. Furthermore, they

demonstrate that new active sites can be accessed by modifying the Cu content, the size of Cu nanoparticles, or the support of the metal catalyst, unraveling novel structure−activity relationships over ZrO_2-supported materials and improving the understanding of the interaction between Cu and ZrO_2, as well as its interdependence with the Cu particle size.

AUTHOR INFORMATION

Corresponding Authors

Tomás Vergara − *Institut für Katalyseforschung und Technologie (IKFT), Karlsruher Institut für Technologie (KIT), Eggenstein-Leopoldshafen 76344, Germany; Carbon and Catalysis Laboratory (CarboCat), Universidad de Concepción, Concepción 4070386, Chile;* orcid.org/0000-0002-7715-1902; Email: tomas.vergara@kit.edu

Alejandro Karelovic − *Carbon and Catalysis Laboratory (CarboCat), Universidad de Concepción, Concepción 4070386, Chile;* orcid.org/0000-0001-5189-0902; Email: akarelov@udec.cl

Authors

Daviel Gómez − *Instituto de Tecnología Química (ITQ), Universitat Politècnica de València-Consejo Superior de Investigaciones Científicas (UPV-CSIC), Valencia 46022, Spain*

Lucas Warmuth − *Institut für Katalyseforschung und Technologie (IKFT), Karlsruher Institut für Technologie (KIT), Eggenstein-Leopoldshafen 76344, Germany;* orcid.org/0000-0002-2234-028X

Annika E. Enss − *Institut für Katalyseforschung und Technologie (IKFT), Karlsruher Institut für Technologie (KIT), Eggenstein-Leopoldshafen 76344, Germany*

Martin Peterlechner − *Laboratory for Electron Microscopy (LEM), Karlsruher Institut für Technologie (KIT), Karlsruhe 76131, Germany*

Rodrigo Pallacán − *Carbon and Catalysis Laboratory (CarboCat), Universidad de Concepción, Concepción 4070386, Chile*

Vlad Martin Diaconescu − *CELLS - ALBA Synchrotron Radiation Facility, Cerdanyola del Vallès 08290, Spain*

Laura Simonelli − *CELLS - ALBA Synchrotron Radiation Facility, Cerdanyola del Vallès 08290, Spain;* orcid.org/0000-0001-5331-0633

Felix Studt − *Institut für Katalyseforschung und Technologie (IKFT), Karlsruher Institut für Technologie (KIT), Eggenstein-Leopoldshafen 76344, Germany;* orcid.org/0000-0001-6841-4232

Patricia Concepción − *Instituto de Tecnología Química (ITQ), Universitat Politècnica de València-Consejo Superior de Investigaciones Científicas (UPV-CSIC), Valencia 46022, Spain;* orcid.org/0000-0003-2058-3103

Romel Jiménez − *Carbon and Catalysis Laboratory (CarboCat), Universidad de Concepción, Concepción 4070386, Chile;* orcid.org/0000-0003-0839-4393

Author Contributions

All authors have given approval to the final version of the manuscript.

Funding

Research Grants−Doctoral Programs in Germany (57645448), awarded by the Deutsche Akademische Austauschdienst (DAAD), Government of Germany. National Agency for Research and Development (ANID), Government of Chile (FONDECYT project number 1221281). Project LINCG23026, CSIC, Ministerio de Ciencia e Innovación, Government of Spain. Helmholtz Research Programme "Storage and Cross-linked Infrastructures", Topic "Synthetic Hydrocarbons", number 380302, Government of Germany.

Notes

The authors declare no competing financial interest.

ACKNOWLEDGMENTS

T.V. acknowledges the financial support from the Research Grants—Doctoral Programs in Germany (57645448), awarded by the Deutsche Akademische Austauschdienst (DAAD), Government of Germany. The authors acknowledge the support given by Sarah Essig for catalyst characterizations and Gabriela Rodrigues Niquini for discussion. XAS experiments were performed at BL22-CLAESS beamline at ALBA Synchrotron, and the authors acknowledge the support given by the ALBA staff Beatriz Moreno, José Soriano and Minjie Zhao. A.E.E. and F.S. acknowledge support by the state of Baden-Württemberg through bwHPC (bwunicluster). The authors acknowledge the financial support from the National Agency for Research and Development (ANID), Government of Chile (FONDECYT project number 1221281), from Universidad de Concepción (UdeC), Chile, from the project LINCG23026, CSIC, Ministerio de Ciencia e Innovación, Government of Spain and from the Helmholtz Research Programme "Storage and Cross-linked Infrastructures", Topic "Synthetic Hydrocarbons", number 380302, Government of Germany.

REFERENCES

(1) Chang, X.; Han, X.; Pan, Y.; Hao, Z.; Chen, J.; Li, M.; Lv, J.; Ma, X. Insight into the Role of Cu−ZrO $_2$ Interaction in Methanol Synthesis from CO $_2$ Hydrogenation. *Ind. Eng. Chem. Res.* **2022**, *61* (20), 6872−6883.

(2) Fisher, I. A.; Bell, A. T. In Situ Infrared Study of Methanol Synthesis from H2/CO over Cu/SiO2and Cu/ZrO2/SiO2. *J. Catal.* **1998**, *178* (1), 153−173.

(3) Fujiwara, K.; Tada, S.; Honma, T.; Sasaki, H.; Nishijima, M.; Kikuchi, R. Influences of Particle Size and Crystallinity of Highly Loaded CuO/ZrO $_2$ on CO $_2$ Hydrogenation to Methanol. *AIChE J.* **2019**, *65* (12), No. e16717.

(4) Lam, E.; Larmier, K.; Tada, S.; Wolf, P.; Safonova, O. V.; Copéret, C. Zr(IV) Surface Sites Determine CH3OH Formation Rate on Cu/ZrO2/SiO2 - CO2 Hydrogenation Catalysts. *Chin. J. Catal.* **2019**, *40* (11), 1741−1748.

(5) Larmier, K.; Liao, W.-C.; Tada, S.; Lam, E.; Verel, R.; Bansode, A.; Urakawa, A.; Comas-Vives, A.; Copéret, C. CO2-to-Methanol

Hydrogenation on Zirconia-Supported Copper Nanoparticles: Reaction Intermediates and the Role of the Metal−Support Interface. *Angew. Chem., Int. Ed.* **2017**, *56* (9), 2318−2323.
(6) Meunier, F. C.; Dansette, I.; Paredes-Nunez, A.; Schuurman, Y. Cu-Bound Formates Are Main Reaction Intermediates during CO_2 Hydrogenation to Methanol over Cu/ZrO_2. *Angew. Chem., Int. Ed.* **2023**, *62* (29), No. e202303939.
(7) Rhodes, M.; Bell, A. The Effects of Zirconia Morphology on Methanol Synthesis from CO and H2H2 over Cu/ZrO2Cu/ZrO2 catalystsPart I. *Steady-State Studies. J. Catal.* **2005**, *233* (1), 198−209.
(8) Rhodes, M.; Pokrovski, K.; Bell, A. The Effects of Zirconia Morphology on Methanol Synthesis from CO and H2 over Cu/ZrO2 catalystsPart II. *Transient-Response Infrared Studies. J. Catal.* **2005**, *233* (1), 210−220.
(9) Ro, I.; Liu, Y.; Ball, M. R.; Jackson, D. H. K.; Chada, J. P.; Sener, C.; Kuech, T. F.; Madon, R. J.; Huber, G. W.; Dumesic, J. A. Role of the Cu-ZrO_2 Interfacial Sites for Conversion of Ethanol to Ethyl Acetate and Synthesis of Methanol from CO_2 and H_2. *ACS Catal.* **2016**, *6* (10), 7040−7050.
(10) Samson, K.; Śliwa, M.; Socha, R. P.; Góra-Marek, K.; Mucha, D.; Rutkowska-Zbik, D.; Paul, J.-F.; Ruggiero-Mikołajczyk, M.; Grabowski, R.; Słoczyński, J. Influence of ZrO_2 Structure and Copper Electronic State on Activity of Cu/ZrO_2 Catalysts in Methanol Synthesis from CO_2. *ACS Catal.* **2014**, *4* (10), 3730−3741.
(11) Tada, S.; Katagiri, A.; Kiyota, K.; Honma, T.; Kamei, H.; Nariyuki, A.; Uchida, S.; Satokawa, S. Cu Species Incorporated into Amorphous ZrO_2 with High Activity and Selectivity in CO_2 -to-Methanol Hydrogenation. *J. Phys. Chem. C* **2018**, *122* (10), 5430−5442.
(12) Tada, S.; Larmier, K.; Büchel, R.; Copéret, C. Methanol Synthesis *via* CO_2 Hydrogenation over $CuO−ZrO_2$ Prepared by Two-Nozzle Flame Spray Pyrolysis. *Catal. Sci. Technol.* **2018**, *8* (8), 2056−2060.
(13) Tada, S.; Kayamori, S.; Honma, T.; Kamei, H.; Nariyuki, A.; Kon, K.; Toyao, T.; Shimizu, K.; Satokawa, S. Design of Interfacial Sites between Cu and Amorphous ZrO_2 Dedicated to CO_2 -to-Methanol Hydrogenation. *ACS Catal.* **2018**, *8* (9), 7809−7819.
(14) Wu, C.; Lin, L.; Liu, J.; Zhang, J.; Zhang, F.; Zhou, T.; Rui, N.; Yao, S.; Deng, Y.; Yang, F.; Xu, W.; Luo, J.; Zhao, Y.; Yan, B.; Wen, X.-D.; Rodriguez, J. A.; Ma, D. Inverse ZrO2/Cu as a Highly Efficient Methanol Synthesis Catalyst from CO2 Hydrogenation. *Nat. Commun.* **2020**, *11* (1), 5767.
(15) Wang, Y. H.; Gao, W. G.; Wang, H.; Zheng, Y. E.; Na, W.; Li, K. Z. Structure−Activity Relationships of $Cu−ZrO_2$ Catalysts for CO_2 Hydrogenation to Methanol: Interaction Effects and Reaction Mechanism. *RSC Adv.* **2017**, *7* (14), 8709−8717.
(16) Zhan, H.; Shi, X.; Tang, B.; Wang, G.; Ma, B.; Liu, W. The Performance of Cu/Zn/Zr Catalysts of Different Zr/(Cu+Zn) Ratio for CO2 Hydrogenation to Methanol. *Catal. Commun.* **2021**, *149*, No. 106264.
(17) Barberis, L.; Hakimioun, A. H.; Plessow, P. N.; Visser, N. L.; Stewart, J. A.; Vandegehuchte, B. D.; Studt, F.; De Jongh, P. E. Competition between Reverse Water Gas Shift Reaction and Methanol Synthesis from CO_2: Influence of Copper Particle Size. *Nanoscale* **2022**, *14* (37), 13551−13560.
(18) Karelovic, A.; Galdames, G.; Medina, J. C.; Yévenes, C.; Barra, Y.; Jiménez, R. Mechanism and Structure Sensitivity of Methanol Synthesis from CO2 over SiO2-Supported Cu Nanoparticles. *J. Catal.* **2019**, *369*, 415−426.
(19) van den Berg, R.; Prieto, G.; Korpershoek, G.; van der Wal, L. I.; van Bunningen, A. J.; Lægsgaard-Jørgensen, S.; de Jongh, P. E.; de Jong, K. P. Structure Sensitivity of Cu and CuZn Catalysts Relevant to Industrial Methanol Synthesis. *Nat. Commun.* **2016**, *7* (1), 13057.
(20) Visser, N. L.; Daoura, O.; Plessow, P. N.; Smulders, L. C. J.; De Rijk, J. W.; Stewart, J. A.; Vandegehuchte, B. D.; Studt, F.; Van Der Hoeven, J. E. S.; De Jongh, P. E. Particle Size Effects of Carbon Supported Nickel Nanoparticles for High Pressure CO_2 Methanation. *ChemCatChem.* **2022**, *14* (22), No. e202200665.
(21) Simons, J. F. M.; De Heer, T. J.; Van De Poll, R. C. J.; Muravev, V.; Kosinov, N.; Hensen, E. J. M. Structure Sensitivity of CO_2 Hydrogenation on Ni Revisited. *J. Am. Chem. Soc.* **2023**, *145* (37), 20289−20301.
(22) Nørskov, J. K.; Bligaard, T.; Hvolbæk, B.; Abild-Pedersen, F.; Chorkendorff, I.; Christensen, C. H. The Nature of the Active Site in Heterogeneous Metal Catalysis. *Chem. Soc. Rev.* **2008**, *37* (10), 2163−2171.
(23) Van Santen, R. A. Complementary Structure Sensitive and Insensitive Catalytic Relationships. *Acc. Chem. Res.* **2009**, *42* (1), 57−66.
(24) Zhang, X.; Liu, J.-X.; Zijlstra, B.; Filot, I. A. W.; Zhou, Z.; Sun, S.; Hensen, E. J. M. Optimum Cu Nanoparticle Catalysts for CO2 Hydrogenation towards Methanol. *Nano Energy* **2018**, *43*, 200−209.
(25) Vergara, T.; Gómez, D.; de Oliveira Campos, B. L.; Delgado, K. H.; Concepción, P.; Jiménez, R.; Karelovic, A. Combined Role of Ce Promotion and TiO2 Support Improves CO2 Hydrogenation to Methanol on Cu Catalysts: Interplay between Structure and Kinetics. *J. Catal.* **2023**, *426*, 200−213.
(26) Soled, S. L.; Malek, A.; Miseo, S.; Baumgartner, J.; Kliewer, C.; Afeworki, M.; Stevens, P. A. Supported Metal Catalysts: Some Interesting New Leads In An Old Field. In *Studies in Surface Science and Catalysis*; Elsevier, 2006; vol *162*, pp 103−110.
(27) Simonelli, L.; Marini, C.; Olszewski, W.; Ávila Pérez, M.; Ramanan, N.; Guilera, G.; Cuartero, V.; Klementiev, K. CLAESS: The Hard X-Ray Absorption Beamline of the ALBA CELLS Synchrotron. *Cogent Phys.* **2016**, *3* (1), No. 1231987.
(28) Ravel, B.; Newville, M. *ATHENA*, *ARTEMIS*, *HEPHAESTUS*: Data Analysis for X-Ray Absorption Spectroscopy Using *IFEFFIT*. *J. Synchrotron Radiat.* **2005**, *12* (4), 537−541.
(29) Kresse, G.; Joubert, D. From Ultrasoft Pseudopotentials to the Projector Augmented-Wave Method. *Phys. Rev. B* **1999**, *59* (3), 1758−1775.
(30) Larsen, A. H.; Mortensen, J. J.; Blomqvist, J.; Castelli, I. E.; Christensen, R.; Dułak, M.; Friis, J.; Groves, M. N.; Hammer, B.; Hargus, C.; Hermes, E. D.; Jennings, P. C.; Jensen, P. B.; Kermode, J.; Kitchin, J. R.; Kolsbjerg, E. L.; Kubal, J.; Kaasbjerg, K.; Lysgaard, S.; Maronsson, J. B.; Maxson, T.; Olsen, T.; Pastewka, L.; Peterson, A.; Rostgaard, C.; Schiøtz, J.; Schütt, O.; Strange, M.; Thygesen, K. S.; Vegge, T.; Vilhelmsen, L.; Walter, M.; Zeng, Z.; Jacobsen, K. W. The Atomic Simulation Environment—a Python Library for Working with Atoms. *J. Phys.: Condens. Matter* **2017**, *29* (27), 273002.
(31) Wellendorff, J.; Lundgaard, K. T.; Møgelhøj, A.; Petzold, V.; Landis, D. D.; Nørskov, J. K.; Bligaard, T.; Jacobsen, K. W. Density Functionals for Surface Science: Exchange-Correlation Model Development with Bayesian Error Estimation. *Phys. Rev. B* **2012**, *85* (23), No. 235149.
(32) Polierer, S.; Jelic, J.; Pitter, S.; Studt, F. On the Reactivity of the Cu/ZrO2 System for the Hydrogenation of CO2 to Methanol: A Density Functional Theory Study. *J. Phys. Chem. C* **2019**, *123* (44), 26904−26911.
(33) Lin, T. C.; Bhan, A. Rates and Reversibility of CO2 Hydrogenation on Cu-Based Catalysts. *J. Catal.* **2024**, *429*, No. 115214.
(34) Lin, T. C.; Razdan, N. K.; Bhan, A. Rates and Reversibilities in Interconnected Reaction Networks. *ACS Catal.* **2022**, *12* (5), 3100−3110.
(35) Vergara, T.; Gómez, D.; de Oliveira Campos, L. B.; Delgado, K. H.; Jiménez, R.; Karelovic, A. Disclosing the Reaction Mechanism of CO_2 Hydrogenation to Methanol over $CuCeO_x/TiO_2$: A Combined Kinetic, Spectroscopic, and Isotopic Study. *ACS Catal.* **2023**, *13* (22), 14699−14715.
(36) Hu, M.; Lu, X.; Zhu, C.; Yang, T.; Tan, H.; Jin, L.; Kerns, P.; Meng, M.; Suib, S. L.; Gao, P.; He, J. Ultrasmall Cu Nanoparticles Supported on Crystalline, Mesoporous ZnO for Selective CO_2 Hydrogenation. *ChemCatChem.* **2023**, *16* (3), No. e202301077.
(37) Yang, B.; Liu, C.; Halder, A.; Tyo, E. C.; Martinson, A. B. F.; Seifert, S.; Zapol, P.; Curtiss, L. A.; Vajda, S. Copper Cluster Size Effect in Methanol Synthesis from CO_2. *J. Phys. Chem. C* **2017**, *121* (19), 10406−10412.
(38) Warmuth, L.; Steurer, M.; Schild, D.; Zimina, A.; Grunwaldt, J.-D.; Pitter, S. Reversible and Irreversible Structural Changes in Cu/

ZnO/ZrO $_2$ Catalysts during Methanol Synthesis. *ACS Appl. Mater. Interfaces* **2024**, *16* (7), 8813−8821.
(39) Studt, F.; Behrens, M.; Abild-Pedersen, F. Energetics of the Water−Gas-Shift Reaction on the Active Sites of the Industrially Used Cu/ZnO/Al2O3 Catalyst. *Catal. Lett.* **2014**, *144* (11), 1973−1977.
(40) Kunkes, E. L.; Studt, F.; Abild-Pedersen, F.; Schlögl, R.; Behrens, M. Hydrogenation of CO2 to Methanol and CO on Cu/ZnO/Al2O3: Is There a Common Intermediate or Not? *J. Catal.* **2015**, *328*, 43−48.
(41) Zhu, J.; Ciolca, D.; Liu, L.; Parastaev, A.; Kosinov, N.; Hensen, E. J. M. Flame Synthesis of Cu/ZnO−CeO $_2$ Catalysts: Synergistic Metal−Support Interactions Promote CH $_3$ OH Selectivity in CO $_2$ Hydrogenation. *ACS Catal.* **2021**, *11* (8), 4880−4892.
(42) Goguet, A.; Meunier, F. C.; Tibiletti, D.; Breen, J. P.; Burch, R. Spectrokinetic Investigation of Reverse Water-Gas-Shift Reaction Intermediates over a Pt/CeO $_2$ Catalyst. *J. Phys. Chem. B* **2004**, *108* (52), 20240−20246.
(43) Wang, W.; Qu, Z.; Song, L.; Fu, Q. CO2 Hydrogenation to Methanol over Cu/CeO2 and Cu/ZrO2 Catalysts: Tuning Methanol Selectivity via Metal-Support Interaction. *J. Energy Chem.* **2020**, *40*, 22−30.
(44) Bando, K. K.; Sayama, K.; Kusama, H.; Okabe, K.; Arakawa, H. In-Situ FT-IR Study on CO2 Hydrogenation over Cu Catalysts Supported on SiO2, Al2O3, and TiO2. *Appl. Catal. Gen.* **1997**, *165* (1), 391−409.
(45) Jung, K.-D.; Bell, A. T. Role of Hydrogen Spillover in Methanol Synthesis over Cu/ZrO2. *J. Catal.* **2000**, *193* (2), 207−223.
(46) Fehr, S. M.; Nguyen, K.; Krossing, I. Realistic *Operando*- DRIFTS Studies on Cu/ZnO Catalysts for CO $_2$ Hydrogenation to Methanol−Direct Observation of Mono-ionized Defect Sites and Implications for Reaction Intermediates. *ChemCatChem.* **2022**, *14* (3), No. e202101500.
(47) Collins, S.; Baltanas, M.; Bonivardi, A. An Infrared Study of the Intermediates of Methanol Synthesis from Carbon Dioxide over Pd/-GaO. *J. Catal.* **2004**, *226* (2), 410−421.
(48) Crampton, A. S.; Rötzer, M. D.; Ridge, C. J.; Schweinberger, F. F.; Heiz, U.; Yoon, B.; Landman, U. Structure Sensitivity in the Nonscalable Regime Explored via Catalysed Ethylene Hydrogenation on Supported Platinum Nanoclusters. *Nat. Commun.* **2016**, *7* (1), 10389.
(49) Stakheev, A. Y.; Kustov, L. M. Effects of the Support on the Morphology and Electronic Properties of Supported Metal Clusters: Modern Concepts and Progress in 1990s. *Appl. Catal. Gen.* **1999**, *188* (1), 3−35.
(50) Vogt, C.; Monai, M.; Kramer, G. J.; Weckhuysen, B. M. The Renaissance of the Sabatier Reaction and Its Applications on Earth and in Space. *Nat. Catal.* **2019**, *2* (3), 188−197.
(51) Cuenya, B. R. Synthesis and Catalytic Properties of Metal Nanoparticles: Size, Shape, Support, Composition, and Oxidation State Effects. *Thin Solid Films* **2010**, *518* (12), 3127−3150.
(52) Ivanova, T. M.; Maslakov, K. I.; Sidorov, A. A.; Kiskin, M. A.; Linko, R. V.; Savilov, S. V.; Lunin, V. V.; Eremenko, I. L. XPS Detection of Unusual Cu(II) to Cu(I) Transition on the Surface of Complexes with Redox-Active Ligands. *J. Electron Spectrosc. Relat. Phenom.* **2020**, *238*, 146878.
(53) Ghodselahi, T.; Vesaghi, M. A.; Shafiekhani, A.; Baghizadeh, A.; Lameii, M. XPS Study of the Cu@Cu2O Core-Shell Nanoparticles. *Appl. Surf. Sci.* **2008**, *255* (5, Part 2), 2730−2734.
(54) Espinós, J. P.; Morales, J.; Barranco, A.; Caballero, A.; Holgado, J. P.; González-Elipe, A. R. Interface Effects for Cu, CuO, and Cu2O Deposited on SiO2 and ZrO2. XPS Determination of the Valence State of Copper in Cu/SiO2 and Cu/ZrO2 Catalysts. *J. Phys. Chem. B* **2002**, *106* (27), 6921−6929.
(55) Nielsen, N. D.; Smitshuysen, T. E. L.; Damsgaard, C. D.; Jensen, A. D.; Christensen, J. M. Characterization of Oxide-Supported Cu by Infrared Measurements on Adsorbed CO. *Surf. Sci.* **2021**, *703*, No. 121725.
(56) Hollins, P.; Pritchard, J. Interactions of CO Molecules Adsorbed on Cu(111). *Surf. Sci.* **1979**, *89* (1−3), 486−495.
(57) Sakakini, B. H.; Tabatabaei, J.; Watson, M. J.; Waugh, K. C. Structural Changes of the Cu Surface of a Cu/ZnO/Al2O3 Catalyst, Resulting from Oxidation and Reduction, Probed by CO Infrared Spectroscopy. *J. Mol. Catal. Chem.* **2000**, *162* (1), 297−306.
(58) Horn, K.; Hussain, M.; Pritchard, J. The Adsorption of CO on Cu(110). *Surf. Sci.* **1977**, *63*, 244−253.
(59) Arena, F.; Italiano, G.; Barbera, K.; Bordiga, S.; Bonura, G.; Spadaro, L.; Frusteri, F. Solid-State Interactions, Adsorption Sites and Functionality of Cu-ZnO/ZrO2 Catalysts in the CO2 Hydrogenation to CH3OH. *Appl. Catal. Gen.* **2008**, *350* (1), 16−23.
(60) Zhao, H.; Yu, R.; Ma, S.; Xu, K.; Chen, Y.; Jiang, K.; Fang, Y.; Zhu, C.; Liu, X.; Tang, Y.; Wu, L.; Wu, Y.; Jiang, Q.; He, P.; Liu, Z.; Tan, L. The Role of Cu1−O3 Species in Single-Atom Cu/ZrO2 Catalyst for CO2 Hydrogenation. *Nat. Catal.* **2022**, *5* (9), 818−831.